Journal of Physics: Conference Series **2919** (2024) 012026 doi:10.1088/1742-6596/2919/1/012026

# Efficient supercontinuum spectra by non-Gaussian pulses

**Chandrika Barman[1]*, Krishanu Lal Mazumder[1], Rohit Mukherjee[2], and Nitu Borgohain[1]**

1Department of Physics, University of Science & Technology Meghalaya, Ri-Bhoi, Meghalaya, India-793101

2Theoretical Photonics Group, Department of Physics, Sarala Birla University, Jharkhand, India-835103

*E-mail: chandrikabarman08@gmail.com

**Abstract.** In this article, we examine the generation of supercontinuum spectra using various non-Gaussian pulses in semiconductor quantum wells. Specifically, we employ weak probe pulses modulated by a strong optical beam, leveraging electromagnetically induced transparency within the system. Our findings indicate that the characteristics of supercontinuum generation, as compared to traditional Gaussian pulses, differ significantly when non-Gaussian pulses, such as sinh-Gaussian, cosh-Gaussian, and tanh-Gaussian pulses are being used. Notably, among the pulses studied, the cosh-Gaussian pulse achieves the broadest supercontinuum span, reaching ~21 μm, at the end of the semiconductor quantum well. These results suggest potential applications in optoelectronic and photonic devices designed for spectroscopic analysis.

## 1. Introduction

Supercontinuum generation (SCG) is a process that produces a broad and continuous spectrum of light, spanning a wide range of wavelengths from a narrow-band input (Zheltikov, 2003; Dudley, 2013). This phenomenon has significant implications for various applications, including spectroscopy, optical coherence tomography, frequency metrology, and telecommunications (Sylvestre, 2021; Tu, 2013). SCG typically occurs when intense laser pulses propagate through a nonlinear medium, causing various nonlinear optical phenomena like self-phase modulation, four-wave mixing, and soliton dynamics.(Ehrlich, 2016). While most studies on SCG have traditionally employed Gaussian pulses, recent advancements have highlighted the potential of non-Gaussian pulses to enhance and control the generated supercontinuum spectra.

Semiconductor quantum wells (SQWs) are particularly attractive for SCG due to their unique electronic and optical properties, which are tunable via quantum confinement (Borgohain, 2016; Borgohain, 2019). These low-dimensional structures exhibit enhanced optical nonlinearities, making them suitable for various advanced photonic applications (Liu, 2017; Wang, 2021). Furthermore, the phenomenon of electromagnetically induced transparency (EIT) in SQWs offers an additional mechanism to control and optimize nonlinear interactions (Phillips, 2018). EIT involves the interaction of a weak probe beam with a strong control beam, leading to a reduction in absorption and the enhancement of nonlinear effects within the medium.

In this study, we explore SCG in MQWs under the influence of EIT. By employing weak probe pulses modulated by a strong optical beam, we leverage EIT to facilitate efficient nonlinear optical interactions in the quantum well structures. This approach not only enhances the nonlinear response but also provides a platform to investigate the influence of various pulse

shapes on SCG. We specifically focus on the generation of supercontinuum spectra using non-Gaussian pulses, including sinh-Gaussian, cosh-Gaussian, and tanh-Gaussian pulses, and compare their performance with traditional Gaussian pulses.

The article's structure unfolds like this: section 2 delves into the theoretical framework and fundamental equations that culminate in the susceptibilities and nonlinear Schrödinger equation, pivotal for examining the dynamics of pulse propagation.

## 2. Theoretical Model and Governing Equations

We consider a multiple quantum well (MQW) as shown in figure1(a). The quantum well configuration was initially presented by Dynes et al. in 2005 (Dynes, 2005), fabricated using molecular beam epitaxy (MBE) to ensure lattice matching on an undoped InP substrate. The sample consists of 30 periods, each with 4.8 nm $In_{0.47}Ga_{0.53}As$, 0.2 nm $Al_{0.48}In_{0.52}As$, and 4.8 nm $In_{0.47}Ga_{0.53}As$ coupled quantum wells, separated by barriers of 36 nm $Al_{0.48}In_{0.52}As$ semiconductor.

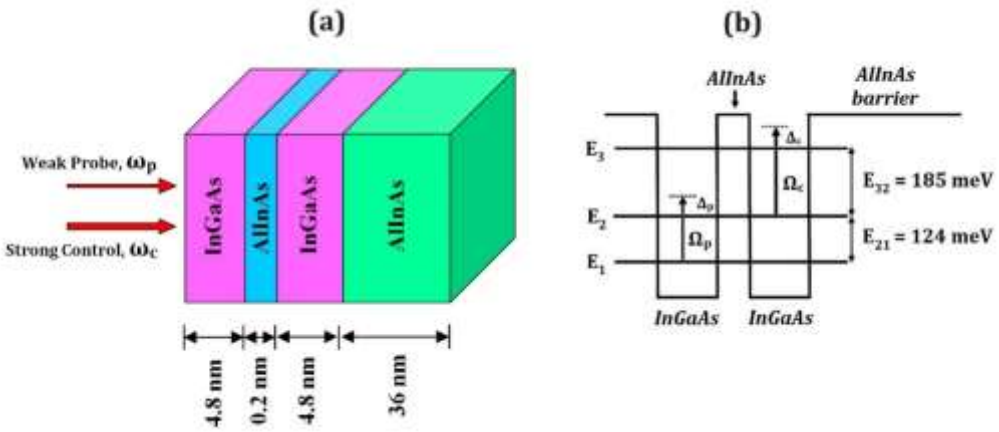


Fig.1: (a) Schematic of the quantum well system, and (b) Energy level diagram with the ladder-like excitation scheme.

As schematically shown in figure 1(b), a ladder type excitation scheme is employed in the system, where a weak probe pulse of frequency $\omega_p$ and amplitude $E_p$ couples the transition between states $|1\rangle$ and $|2\rangle$ and a strong control laser beam of frequency $\omega_c$ and amplitude $E_c$ couples the transition between states $|2\rangle$ and $|3\rangle$.

The Hamiltonian of the system can be written as,

$$\hat{H} = \sum_{i=1}^{3} E_i|i\rangle\langle i| + -\hbar\{\Omega_p e^{i(k_p z-\omega_p t)}|2\rangle\langle 1| + \Omega_c e^{i(k_c z-\omega_c t)}|3\rangle\langle 2| + h.c.\}, \quad (1)$$

where the first term denotes the free Hamiltonian in the absence of any external field and the second term is the perturbed Hamiltonian due to the interaction between the fields and the MQW. The half Rabi frequencies of the probe and the control fields are defined as, $\Omega_p = \frac{(\hat{\mu}_{21}.\hat{e}_p)E_p}{2\hbar}$ and $\Omega_c = \frac{(\hat{\mu}_{23}.\hat{e}_c)E_c}{2\hbar}$ , respectively, where $\hat{\mu}_{jk} = e\langle j|z|k\rangle$ is the dipole matrix element for the transition $|j\rangle \leftrightarrows |k\rangle$. We use the density matrix formalism (Scully, 1997) to investigate the light-matter interaction process in the MQW, which leads to the following rate equations:

$$\dot{\tilde{\rho}}_{21} = i\left(\Delta_p + i\frac{\gamma_{21}}{2}\right)\tilde{\rho}_{21} + i\Omega_p(\tilde{\rho}_{11} - \tilde{\rho}_{22}) + i\Omega_c^*\tilde{\rho}_{31}\,, \tag{2}$$

$$\dot{\tilde{\rho}}_{32} = i\left(\Delta_c + i\frac{\gamma_{32}}{2}\right)\tilde{\rho}_{32} + i\Omega_c(\tilde{\rho}_{22} - \tilde{\rho}_{33}) - i\Omega_p^*\tilde{\rho}_{31}\,, \tag{3}$$

$$\dot{\tilde{\rho}}_{31} = i\left(\Delta_p + \Delta_c + i\frac{\gamma_{31}}{2}\right)\tilde{\rho}_{31} + i\Omega_c\tilde{\rho}_{21} - i\Omega_p\tilde{\rho}_{32}\,, \tag{4}$$

where $\gamma_{jk}(j \neq k)$ represents the total coherence relaxation rates which includes both quasi-elastic acoustic phonon scattering and elastic interface Raman scattering. The detunings $\Delta_p$ and $\Delta_c$ can be expressed as $\Delta_p = \omega_p - \omega_{21}$ and $\Delta_c = \omega_c - \omega_{32}$ , where $\omega_{kj}(j \neq k)$ are the angular frequencies between the states $|j\rangle \leftrightarrows |k\rangle$.

The susceptibility $\chi_p$ contains both linear and non-linear susceptibility and can be expressed as,

$$\chi_p = \chi^{(1)} + \chi^{(3)}\left|E_p\right|^2 + \cdots, \tag{5}$$

where $\chi^{(1)}$ and $\chi^{(3)}$ are the first and third order susceptibilities respectively and can be expressed as,

$$\chi^{(1)} = -\frac{N|\mu_{12}|^2}{\hbar\varepsilon_0}\frac{D_p(0)}{D(0)}, \tag{6}$$

$$\chi^{(3)} = \frac{N|\mu_{12}|^4}{4\hbar^3\varepsilon_0}\frac{\left(|\Omega_c|^2 + \left|D_p(0)\right|^2\right)D_p(0)}{|D(0)|^2 D(0)}, \tag{7}$$

where $D_p(0) = \left(\Delta_p + \Delta_c + i\frac{\gamma_{31}}{2}\right)$, and $D(0) = \left(\Delta_p + i\frac{\gamma_{21}}{2}\right)\left(\Delta_p + \Delta_c + i\frac{\gamma_{31}}{2}\right) - |\Omega_c|^2$. We limit our investigation to the third-order susceptibility and disregard higher-order terms.By following the standard methodology, the propagation constant $\beta(\omega)$can be expressed as,

$$\beta(\omega) = \frac{\omega}{c} - \kappa\frac{D_p(\omega)}{D(\omega)} \tag{8}$$

The propagation constant $\beta(\omega)$can be expressed using a Taylor series expansion centered around the central frequency of the pump field ($\omega = 0$)as follows,

$$\beta(\omega) = \beta(0) + \beta_1(0)\omega + \frac{1}{2}\beta_2(0)\omega^2 + \frac{1}{6}\beta_3(0)\omega^3 + \cdots, \tag{9}$$

where $\beta_n(0) = \left.\frac{d^n\beta(\omega)}{d\omega^n}\right|_{\omega=0}$. Thus we have,

$$\beta(0) = -\frac{\kappa D_p(0)}{D(0)} \tag{10}$$

$$\beta_1(0) = \frac{1}{c} - \frac{\kappa}{D(0)} + \frac{\kappa D_p(0)\left(2\Delta_p + \Delta_c + i\frac{\gamma_{31}}{2} + i\frac{\gamma_{21}}{2}\right)}{\{D(0)\}^2} \tag{11}$$

$$\beta_2(0) = \frac{2\kappa\left(2\Delta_p + \Delta_c + i\frac{\gamma_{31}}{2} + i\frac{\gamma_{21}}{2}\right)}{\{D(0)\}^2} - \frac{2\kappa\left(2\Delta_p + \Delta_c + i\frac{\gamma_{31}}{2} + i\frac{\gamma_{21}}{2}\right)\left(\Delta_p + \Delta_c + i\frac{\gamma_{31}}{2}\right)}{\{D(0)\}^3} + \frac{2\kappa D_p(0)}{\{D(0)\}^2} \tag{12}$$

$$\beta_3(0) = \frac{6\kappa}{|\Omega_c|^2} - \left(\Delta_p + \omega + i\frac{\gamma_{21}}{2}\right)\{D_p(0)\}^2 + \frac{6\kappa\left(2\Delta_p + \Delta_c + i\frac{\gamma_{31}}{2} + i\frac{\gamma_{21}}{2} + 2\omega\right)^2}{\left\{|\Omega_c|^2 - \left(\Delta_p + \omega + i\frac{\gamma_{21}}{2}\right)D_p(0)\right\}^3} +$$

$$\frac{4\kappa\{D_p(0)\}\left(2\Delta_p + \Delta_c + i\frac{\gamma_{31}}{2} + i\frac{\gamma_{21}}{2} + 2\omega\right)}{\left\{|\Omega_c|^2 - \left(\Delta_p + \omega + i\frac{\gamma_{21}}{2}\right)D_p(0)\right\}^3} + \frac{2\kappa\{D_p(0)\}\left(8\Delta_p + 4\Delta_c + i\frac{\gamma_{31}}{2} + i\frac{\gamma_{21}}{2} + 8\omega\right)}{\left\{|\Omega_c|^2 - \left(\Delta_p + \omega + i\frac{\gamma_{21}}{2}\right)D_p(0)\right\}^3} + \frac{6\kappa\{D_p(0)\}\left(2\Delta_p + \Delta_c + i\frac{\gamma_{31}}{2} + i\frac{\gamma_{21}}{2} + 2\omega\right)^3}{\left\{|\Omega_c|^2 - \left(\Delta_p + \omega + i\frac{\gamma_{21}}{2}\right)D_p(0)\right\}^4} \tag{13}$$

The terms $\beta_1(0)$ and $\beta_2(0)$ contributes to the group velocity and group velocity dispersion of the pump pulse, respectively, resulting in alterations to the pulse's shape during propagation, while $\beta_3(0)$ induces further broadening of the pulse.

We employ the following nonlinear Schrödinger equation to analyze the dynamics of pulse propagation within the system (Fibich, 2015).

$$i\frac{\partial A}{\partial \xi} - \frac{1}{2}\beta_2(0)\frac{\partial^2 A}{\partial T^2} - \frac{i}{6}\beta_3(0)\frac{\partial^3 A}{\partial T^3} - \gamma|A|^2 A = 0, \tag{14}$$

where $= \frac{\hbar\left(\frac{cn\varepsilon_0 S}{2}\right)^{1/2}}{\mu_{12}}\Omega_p$, and $\gamma = \left(\mu_{12}/\hbar\sqrt{\frac{cn\varepsilon_0 S}{2}}\right)^2$, with n and S representing the linear refractive index of the medium and cross-sectional area of the pump laser pulse, respectively. The modified nonlinear Schrödinger equation, which incorporates second- and third-order dispersions and Kerr nonlinearity, is represented by the equation (14). Therefore, equation (14) enables numerical investigation into how group velocity dispersion, third-order dispersion, and self-phase modulation (SPM) induced by nonlinearity collectively affect the system.

## 3. Results and Discussion

### *3.1 Pulse Forms*

In this section we quantitatively investigate the dispersion and nonlinearity exhibited by the MQW. To proceed with, we first consider the following system parameters: $N = 10^{22}m^{-3}$, $\mu_{12} = 23.35\ e\mathring{A}$, $\kappa = 4.69 \times 10^{17}m^{-1}s^{-1}$, and the decay rates $\gamma_{21} = 0.5 \times 10^{12}s^{-1}, \gamma_{31} = 1.0 \times 10^{12}s^{-1}$. The angular frequency of the probe pulse is $\omega_p = 18.92 \times 10^{13}s^{-1}$, which correspond to the probe wavelength $\lambda_p = 9.96\ \mu m$. At this wavelength the dispersion parameters are found to be $\beta_1(0) = 3.35 \times 10^{-9}sm^{-1}$, $\beta_2(0) = -1.05 \times 10^{-20}s^2m^{-1}$ and $\beta_3(0) = 1.10 \times 10^{-33}s^3m^{-1}$ and nonlinear coefficient is turn out to be $\gamma = 1.22 \times 10^5 W^{-1}m^{-1}$, which can be utilized in the simulation for SCG. We choose three different non-Gaussian pulses to launch in the MQW system for the study of SCG, *viz.* sinhyperbolic Gaussian pulse (Konar, 2004) of the form $A = A_0 sinh(\Omega_0 T)exp[-T^2/2T_0^2]$, coshyperbolic Gaussian pulse (Borgohain, 2016) of the form $A = A_0 cosh(\Omega_0 T)exp[-T^2/2T_0^2]$, and tanhyperbolic Gaussian pulse (Sharma, 2022) of the form $A = A_0[1 - tanh(\Omega_0\tau)]exp[-T^2/2T_0^2]$. Here, $\Omega_0$ is a pulse parameterwhich determines the shape of the pulse, $T$ is the temporal width and $T_0$ is associated with the full with at half maximum (FWHM) of the pulse. Since the characteristics of the Gaussian pulse are well known (Agrawal, 2007), so, it is also kept under study for the sake of comparison. The Gaussian pulses can be expressed as $A = A_0 exp[-T^2/2T_0^2]$. Figure 2 depicts the shapes of the four different pulses as mentioned above. For all non-Gaussian cases the pulse parameter is taken to be $\Omega_0 = 1$. Now we are in a position to study the propagation dynamics of these pulses in the MQWs.

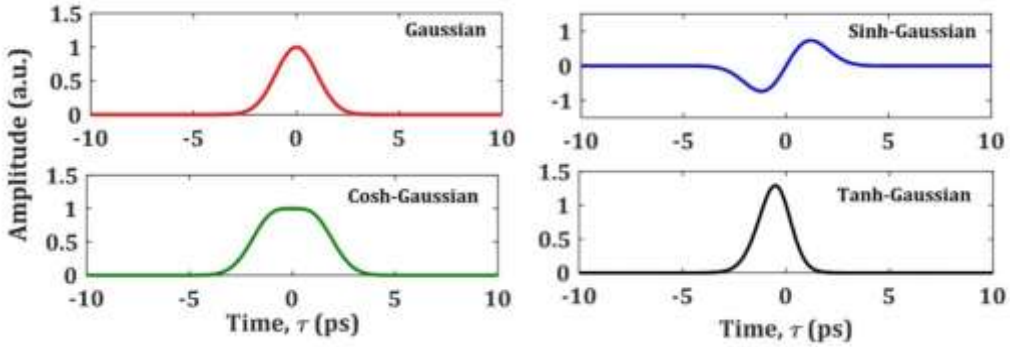


Fig. 2: Plot of Gaussian and various non-Gaussian pulse forms used for the study of SCG in the MQW.

### *3.2 Supercontinuum Generation*

At this stage, we employ numerical simulation to explore the phenomenon of SCG by utilizing the large nonlinearity and low dispersion, mentioned in the previous section, within the MQW.To explore the SCG using numerical simulation, we launch the pulses with FWHM pulse duration of 500 femtosecond and peak power of 500W, injected at probe wavelength 9.96 μm. Figure 3 illustrates the density plots of the spectral and temporal pulses as they travel through the distance of the MQW. These density plots offer valuable insights into the dynamics of propagation and are displayed using a logarithmic density scale limited to -40 dB relative to the maximum value. From the spectral profiles, as depicted in figure 3(a), it is seen that for all the pulses, initial broadening is dominated by nonlinearity induced SPM, as evident from the oscillatory spectrum. Later, the pulses are found to be expanded more because of dispersion and nonlinearity interplayed phenomena like MI, Self-steepening, and soliton generation. The temporal profiles, which are presented in figure 3(b), also depicts that the pulses at initial distances are not broadened, but later, they get extended more towards the positive side in the temporal domain, because of dispersive wave generation, soliton propagation etc.

Next, we focus on the SC spectra generated by different pulses at the end of the MQW, which are presented in figure 4. From the spectral profiles presented in figure 4(a), it is observed that, though the spectra are different from each other, but a common fact is that all are composed of large number of oscillations primarily dominated by nonlinearity induced SPM. The extension of the spectra towards higher wavelength side is attributed by other nonlinearity and dispersion induced effects like MI, soliton generation, etc. The temporal profiles also appear different for different pulses, as presented in fig 4(b), but commonly, there is a prominent soliton peak around the middle of each pulse. Comparing the spectra, it is inferred that the coshyperbolic Gaussian pulse produces the widest spanning of around 21 μm. Thus, among these pulses, the coshyperbolic Gaussian one could be a great option for different spectroscopic or metrological applications of the MQWs in nonlinear optical devices.

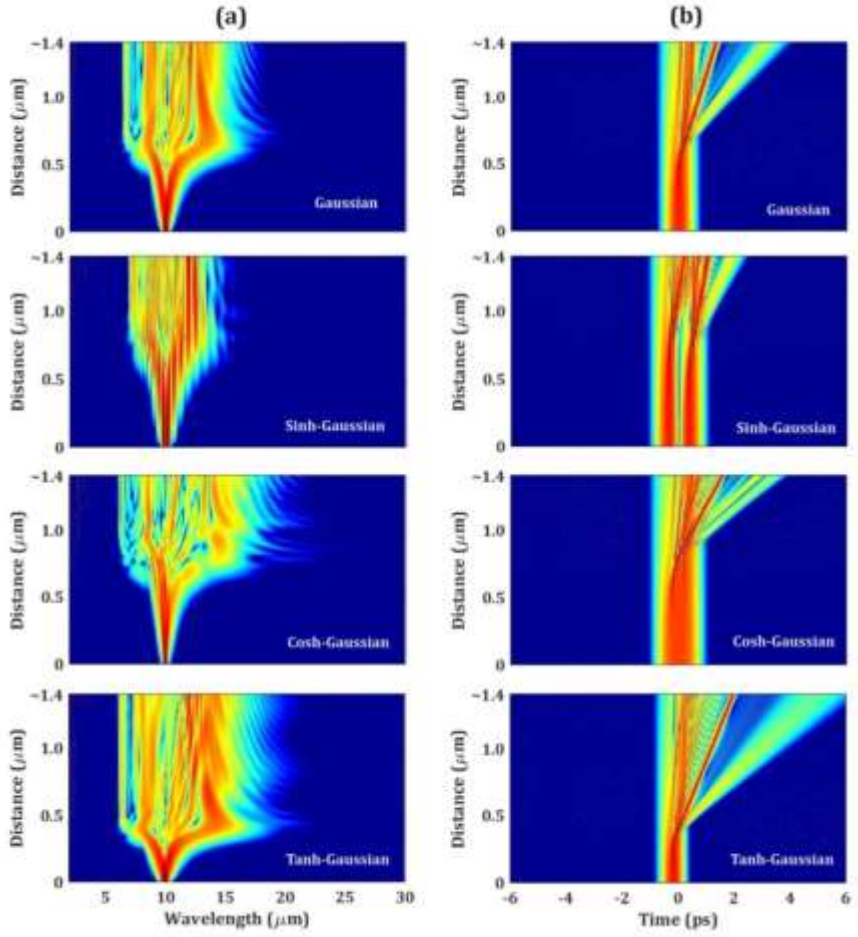


Fig. 3: Density plots illustrating the propagation of the pulses of width 500 fswith peak power of 500W in (a) spectral and (b) temporal domains.

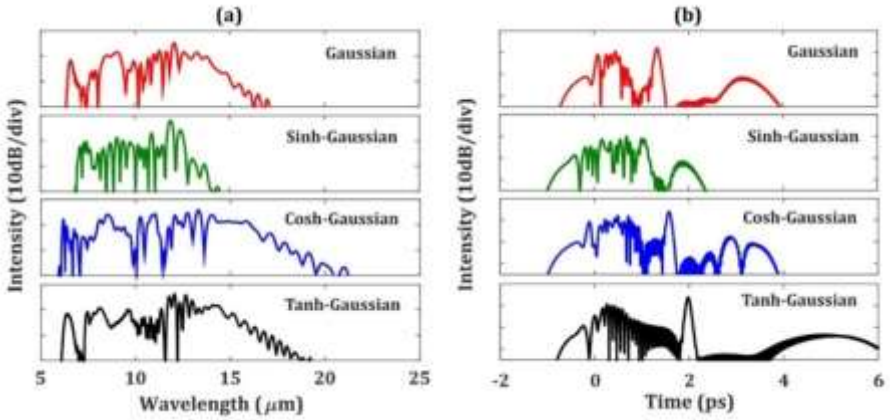


Fig. 4: Slices of supercontinuum spectra of the different pulses at the output of the ~1.4μm long MQW. (a) Spectral, and (b) temporal profiles of the pulse.

## 4. Conclusion

We examined supercontinuum generation within MQW employing different non-Gaussian pulse shapes, including sinh-Gaussian, cosh-Gaussian, and tanh-Gaussian. The pump pulses with peak power of 500W, and FWHM pulse duration of 500fs is launched at wavelength of 9.963μm. Our findings suggest considerable spectral widening primarily driven by phenomena such as self-phase modulation, modulation instability, soliton formation, and dispersive wave generation. Among these, the cosh-Gaussian pulse exhibited the most extensive spectral span, approximately of 21μm. Consequently, cosh-Gaussian pulses for supercontinuum generation promises potential applications in optoelectronic and photonic devices.

## References

Agrawal, G., 2007. *Nonlinear fiber optics.* Ch.3 ed. USA: Nonlinear fiber optics.

Borgohain, N., Belić, M. and Konar, S., 2016. Infrared supercontinuum generation in multiple quantum well nanostructures. *Journal of Optics*, *18*(11), p.115001.

Borgohain, N. and Konar, S., 2019. Broadband mid-infrared supercontinuum generation in three-level multiple quantum wells using short optical pulses. *Optics & Laser Technology*, *120*, p.105684.

Borgohain, N., Sharma, M. and Konar, S., 2016. Broadband supercontinuum generation in photonic crystal fibers using cosh-Gaussian pulses at 835 nm wavelength. *Optik*, *127*(4), pp.1630-1634.

Dudley, J.M. and Genty, G., 2013. Supercontinuum light. *Physics today*, *66*(7), pp.29-34.

Dynes, J.F., Frogley, M.D., Rodger, J. and Phillips, C.C., 2005. Optically mediated coherent population trapping in asymmetric semiconductor quantum wells. *Physical Review B*, *72*(8), p.085323.

Ehrlich, H., Maldonado, M., Parker, A.R., Kulchin, Y.N., Schilling, J., Koehler, B., Skrzypczak, U., Simon, P., Reiswig, H.M., Tsurkan, M.V. and Brunner, E., 2016. Supercontinuum generation in naturally occurring glass sponges spicules. *Advanced Optical Materials*, *4*(10), pp.1608-1613.

Fibich, G., 2015. *The nonlinear Schrödinger equation* (Vol. 192). Berlin: Springer.

Konar, S. and Jana, S., 2004. Linear and nonlinear propagation of sinh-Gaussian pulses in dispersive media possessing Kerr nonlinearity. *Optics communications*, *236*(1-3), pp.7-20.

Liu, X., Guo, Q. and Qiu, J., 2017. Emerging low-dimensional materials for nonlinear optics and ultrafast photonics. *Advanced Materials*, *29*(14), p.1605886.

Phillips, M.C. and Wang, H., 2018. Electromagnetically Induced Transparency in Semiconductor Quantum Wells. In *Non-Equilibrium Dynamics of Semiconductors and Nanostructures* (pp. 215-249). CRC Press.

Scully, M.O. and Zubairy, M.S., 1997. *Quantum optics*. Cambridge university press.

Sharma, M., Kumar, A., Nath, M., Mishra, M. and Borgohain, N., 2022. Enhanced supercontinuum by tan-hyperbolic Gaussian pulses. *Journal of Nanophotonics*, *16*(2), pp.026007-026007.

Sylvestre, T., Genier, E., Ghosh, A.N., Bowen, P., Genty, G., Troles, J., Mussot, A., Peacock, A.C., Klimczak, M., Heidt, A.M. and Travers, J.C., 2021. Recent advances in supercontinuum generation in specialty optical fibers. *JOSA B*, *38*(12), pp.F90-F103.

Tu, H. and Boppart, S.A., 2013. Coherent fibersupercontinuum for biophotonics. *Laser & photonics reviews*, *7*(5), pp.628-645.

Wang, G., Mei, S., Liao, J., Wang, W., Tang, Y., Zhang, Q., Tang, Z., Wu, B. and Xing, G., 2021. Advances of Nonlinear Photonics in Low-Dimensional Halide Perovskites. *Small*, *17*(43), p.2100809.

Zheltikov, A., 2003. Supercontinuum generation. *Applied Physics B*, *77*(2), pp.143-147.